First Attempt at Photoionized Plasma Production with VUV Radiation in Synchrotron Light Source UVSOR-III

Masahiro KOBAYASHI[*,1)], Shinji YOSHIMURA[1)], Hiroshi IWAYAMA[2)], Naonori KONDO[2)], Jun-ichi TAKAHASHI[3,a)], Hiroshi OTA[2)], Masahiro KATOH[2,4)], Kensei Kobayashi[3)] and Hiroaki NAKAMURA[1)]

[1)]*National Institute for Fusion Science, Toki 509-5292, Japan*
[2)]*UVSOR Synchrotron Facility, Institute for Molecular Science, Okazaki 444-8585, Japan*
[3)]*Yokohama National University, Yokohama 240-8501, Japan*
[4)]*Hiroshima Synchrotron Radiation Center, Hiroshima University, Higashi-Hiroshima 739-0046, Japan*

(Received 6 April 2024 / Accepted 1 July 2024)

Photoinduced processes such as photoionization and photoexcitation in the vacuum ultra violet (VUV) energy range are considered important for the divertor region in nuclear fusion reactors and in interstellar space because the cross sections (photoionization, photoexcitation) of these processes in relevant species (hydrogen, helium, neon, argon, and biomolecules) become large in that energy range. Herein, a photoionization experiment was conducted for the first time in the synchrotron light source UVSOR-III with VUV photon energies. The synchrotron light source has the advantage of capability to change photon energy continuously over a wide range and high beam repetition rates. These features allow the simulation of the divertor region and interstellar radiation field to systematically investigate photoinduced processes. Using argon as the sample gas, plasma production was evidenced by the detection of electron current in Langmuir probe measurements. Although an accurate evaluation of the plasma parameters was challenging because of the large scatter of probe data, the possible ranges of plasma parameters are discussed based on a 0 D model of photoionization plasmas [R.M. van der Horst *et al.*, J. Phys. D: Appl. Phys. **48**, 285203 (2015)] and a newly proposed 1 D model in the steady state. Analysis result indicates that plasma density is in the range of 10^{10} - 10^{11} m^{-3}. Additionally, the further development of experiments is discussed for realizing higher plasma densities and for studying photoinduced processes in the divertor region in nuclear fusion reactors and interstellar plasma in terms of the chemical evolution of biomolecules.

Keywords: photoionization, synchrotron light source, plasma, divertor, nuclear fusion, astrobiology

DOI: 10.1585/pfr.19.1301028

In nuclear fusion reactors, the densities of plasmas and neutral hydrogen in the divertor region increase by more than one order of magnitude compared with present-day devices [1]. Simultaneously, photon emissions from plasmas in the confinement region (e.g., Bremsstrahlung) and in the scrape-off layers (SOL) (line emissions from highly charged ions introduced auxiliary to induce detachment) increase over a wide wavelength range spanning the extreme ultraviolet (EUV) to the visible and infrared range, because of the higher plasma density required to sustain nuclear fusion reactions. This situation is expected to enhance interactions between hydrogen atoms/molecules, auxiliary ions, and photons in the divertor region. These interactions include the photoionization, photodissociation, and the photoexcitation (electronically, vibrationally, and rotationally). While the effects of photoinduced processes are negligible in modern-day fusion experiments, atomic/molecular processes, which play an important role especially in the low-temperature range below ~10 eV in so-called detached plasmas [2, 3], will be altered in future reactors because of an increase in number of photon.

Meanwhile, partially ionized plasmas exist in interstellar space, where the ionization energy source is cosmic rays or the interstellar radiation field [4]. In this context, photon-induced processes are crucial in the chemical evolution of prebiotic molecules, which are considered to be the origin of life in space [5, 6]. Furthermore, photoinduced processes are important in the earth's ionosphere, where solar radiation in the EUV–VUV energy range interact with oxygen and nitrogen gases to generate weakly ionized plasmas. The collective phenomenon of plasmas under the effects of magnetic and electric fields will exert additional effects on divertor plasmas, the chemical evolution of biomolecules, and the ionosphere. Nevertheless, the characteristics and roles of photoionized plasmas on the divertor operation, the chemical evolutions are not yet fully understood.

[*] *Corresponding author's e-mail: kobayashi.masahiro@nifs.ac.jp*
[a)] *Current affiliation: Graduate School of Maritime Sciences, Kobe University, Kobe 658-0022, Japan*

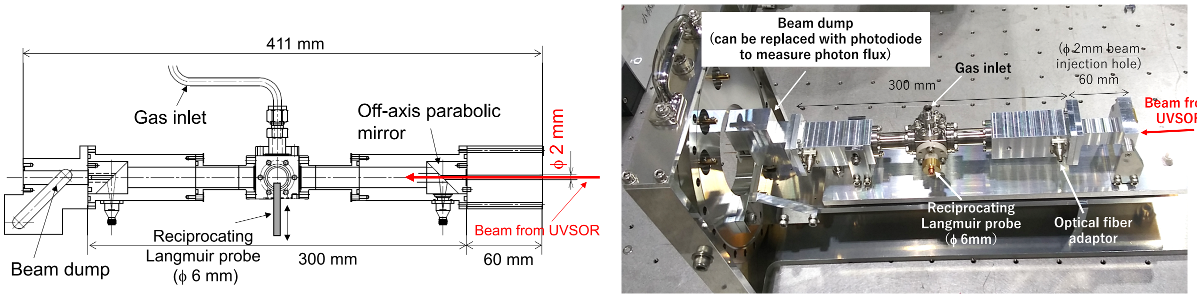

Fig. 1 Schematic and a photo of the gas cell used for photoionization experiments at UVSOR-III.

Photoionization experiments have been conducted mainly for the purpose of EUV lithography [7, 8]. The light source, typically a xenon or tin plasma, involves either applying an electric field via an electrode bias [7] or evaporation via Nd:YAG laser pulse irradiation [8]. In that case, however, the wavelength (photon energy) of the light source is limited to the available spectra of the xenon or tin plasmas.

In contrast, a synchrotron light source can continuously change the wavelength of the light over a wide range, encompassing the X-ray, EUV, VUV, visible, and infrared ranges. In particular, the photoexcitation and photoionization rate coefficients become large at several tens of eV (100 to ~20 nm) for species relevant to nuclear fusion and astrobiology, such as hydrogen, helium, neon, argon, carbon, nitrogen [9], and biomolecules [10]. However, this energy range has not been investigated in detail experimentally, particularly in terms of plasma, as collective phenomena exhibited by charged particles. Meanwhile, the development of gas cell reactor to study the photo-induced process with the synchrotron light source will, therefore, expand the research capability in this field significantly. In these contexts, we are developing an experimental apparatus that can generate photoionized plasmas using the synchrotron light source UVSOR-III in Institute for Molecular Science, Japan [11].

This letter presents a first attempt to generate photoionized plasma using the UVSOR-III synchrotron light source in the VUV energy range.

The BL7B beamline of UVSOR-III was used to generate light in the range of 30 - 500 nm (2.5 - 41 eV). The beam was collimated to a diameter of approximately 1 mm at the center of the vacuum irradiation chamber. A gas cell was installed inside the irradiation chamber to maintain a high pressure of sample gas while maintaining good vacuum condition in the beamline (10^{-6} - 10^{-7} Pa).

Figure 1 shows the gas cell used in the experiments. The length of the gas cell along the beam axis is 300 mm. The length of the cell is made as long as possible to increase interaction volume between the gas and beam. The inner cell diameter was 16 mm. The beam from BL7B is injected into the cell through a hole at the front end (ϕ 2 mm and 60 mm length). The beam was dumped at the end of the gas cell after undergoing multiple reflections from carbon-coated plates to avoid photoelectron emission from the stainless-steel cell wall.

A copper electrode (6 mm diameter) was inserted into the gas cell and biased to +/− 20 V to measure the probe current of the plasmas through a choice of resistors. The bias voltage was applied using dry cell batteries to avoid electrical noise from a power supply. The gas was fed to the cell through an input terminal at the top of the cell. The gas flow rate was controlled by a needle valve. The maximum pressure inside the gas cell was of the order of 1 Pa while the pressure in the irradiation chamber outside the gas cell and upstream along the beam line were kept at values of the order of 10^{-4} and 10^{-7} Pa, respectively. Argon (with ionization potential 14.5 eV) was introduced as the sample gas.

An off-axis silver-coated parabolic mirror was installed at the front end of the gas cell and used to collect the emission from the gas. The beam from the BL7B passes through a 3-mm-diameter hole at the mirror center so that the mirror collected the emission along the beam axis but outside the beam. The parabolic mirror focused the collected emission onto an optical fiber, which was connected to the outside of the vacuum chamber via a vacuum feedthrough and to a spectrometer (Acton Research Corporation, SpectraPro-300i; 0.3 m focal length; CCD: PyLoN 400BRX-UV-LF).

The photon flux of the BL7B was measured with a photodiode (AXUV100G, OptoDiode Corporation) installed at the end of the gas cell, with replacement of the beam dump during the measurements. Figure 2 shows the photon flux detected using the photodiode for different gratings of the beam line. Prior to the experiments, we tested gas cells with different hole sizes for their photon-flux throughput. We found that the photon flux decreased significantly for hole diameters less than 2 mm. This may be due to an interference of the beam by the inner hole surface. The hole configuration (diameter and length) selected in this study was a compromise between the conductance of the gas cell and photon-flux throughput. The throughput of the photon flux in the present gas cell is estimated to be between 10^9 and 10^{10} photons/s in the VUV range as shown in Fig. 2.

Table 1 Parameters of photoionization experiments in various devices. σ_{pi}, n_a, E_{pulse}, A_{beam}, E_{ph}, and n_e^{max} denote the photoionization cross section, neutral atom density, beam-pulse energy, beam cross section, photon energy, and maximum electron density obtained using Eq. (2), respectively. *Estimated for 1 ms pulse. **Estimated from [8].

	Repetition rate (Hz)	Pulse duration	Beam radius	A_{beam} (m^2)	E_{pulse}	$E_{ph}(eV)$	$\sigma_{pi}(m^2)$	Gas pressure (Pa)	$n_a(m^{-3})$	$n_e^{max}(m^{-3})$
ASML [7]	500	150 ns	2 mm	1.3x10^{-5}	53µJ	92 (~13.5 nm)	1.1x10^{-22} (Ar)	1~10	2.1x10^{20}~10^{21}	6.6x10^{15}~10^{16}
ILE [8]	10	10 ns	175 µm**	9.6x10^{-8}	8mJ	103.5 (~12 nm)	4.3x10^{-24} (H)	5	1.0x10^{21}	2.2x10^{19}
UVSOR (BL7B, G2)	90M	< 1 ns	1 mm	3.1x10^{-6}	17pJ*	14.5 (~85.5 nm)	5.0x10^{-21} (Ar)	~1	2.1x10^{20}	2.4x10^{12}
UVSOR (BL1U)	90M	< 1 ns	1 mm	3.1x10^{-6}	0.24~2.4µJ*	14.5 (~85.5 nm)	5.0x10^{-21} (Ar)	1~10	2.1x10^{20}	10^{16}~10^{17}

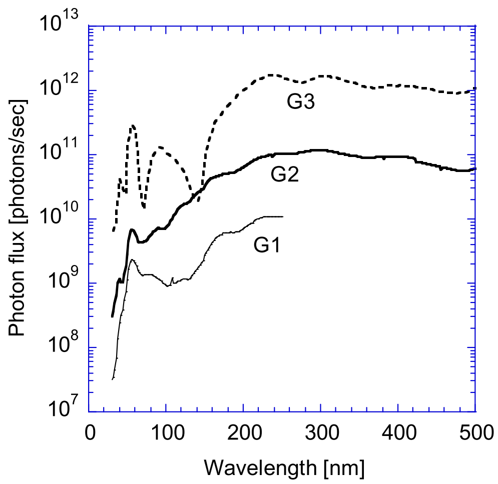

Fig. 2 Photon-flux throughput measured at the end of the gas cell in the beamline BL7B with different gratings.

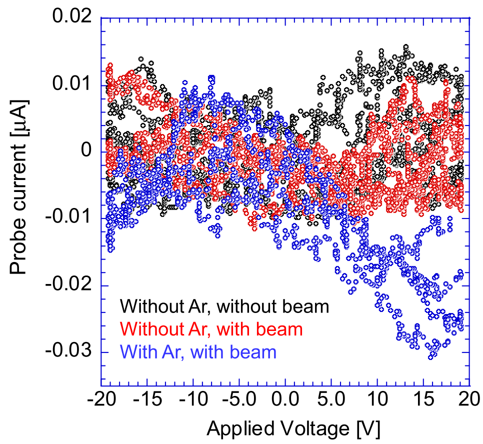

Fig. 3 Probe current as a function of bias voltage for three cases: without Ar and beam (black), without Ar and with beam (red), with Ar and beam (blue). The probe surface is located 4 mm away from the beam axis.

The probe electrode surface was positioned 4 mm away from the beam axis, and current was measured by applying a bias voltage with a 12-kΩ resistor. For this measurement, the zeroth-order light produced using the G2 grating of the beam line was introduced into the gas cell. The probe current is plotted in Fig. 3 for three cases: without argon gas and the beam, without argon gas and with the beam, and with argon gas and the beam, respectively. Due to the very low current the scatter of the data is significant. There is also oscillation of approximately ±0.01 µA around 0 µA for all cases. Nevertheless, a clear negative current is observed under the positive bias in the case with argon and the beam, while in the other two cases, no clear change is noted against the voltage scan within the scatter. As discussed below, we expect the ion saturation current to be undetectable in the present experiments because of the very low degree of ionization of argon gas. Therefore, we corrected the offset of the current under the negative bias such that the averaged current at the zero bias voltage becomes zero. In the case of with argon gas and the beam, the maximum negative current under the positive bias is approximately 0.03 µA. This value is interpreted as electron saturation current, I_e. Due to the large scatter in data, it was difficult to evaluate the electron temperature from the Fig. 3. Below, instead, we discuss the range of the plasma parameters for the present experiments in terms of the photoionization process.

The maximum plasma density produced by photoionization can be estimated using the 0 D model proposed in Ref. [7],

$$n_e^{max} = \frac{\sigma_{pi} n_a E_{pulse}}{A_{beam} E_{ph}}, \tag{1}$$

where $\sigma_{pi}, n_a, E_{pulse}$, A_{beam}, and E_{ph} are the photoionization cross section, neutral atom density, beam pulse energy, the beam cross section, and photon energy, respectively. The parameters of the BL7B are listed in Table 1 together with those from AMSL [7] and ILE [8]. Equation (1) gives $n_e^{max} \approx 2.4 \times 10^{12}$ m^{-3} for BL7B.

Equation (1) has been derived for maximum density that can be achieved transiently during or after the beam pulse. In AMSL and ILE, the pulse duration (of the order of 10 - 100 ns) and repetition rate (10 - 500 Hz) of the light source depend on the duty cycle of the plasma production in the light source. Considering the lifetime (confinement time) of the photoionized plasmas (typically of the order of several hundred microseconds [7], the light source is insufficient to sustain the plasma in the steady state, and therefore only transient phenomena can be studied. However, the radiation fields in nuclear fusion reactors and in space are in the steady state. Furthermore, the repetition rate of the beam in UVSOR-III is 90.1 MHz (with each beam pulse lasting less than 1 ns), which makes it possible to sustain the plasma in the steady state, taking into account the lifetime of the plasma as mentioned above. In this case, a steady-state 1 D transport model along the beam axis can be described as

$$\frac{\partial}{\partial z}(n_i v_i) = S_p - n_i n_e \langle \sigma v \rangle_{rec}, \tag{2}$$

where n_i, n_e, v_i, and $\langle \sigma v \rangle_{rec}$ respectively denote the ion density, electron density, ion flow speed along the beam axis, and recombination-rate coefficient of the ion. S_p is the photoionization source, described as

$$S_p(z) = \frac{\partial}{\partial z}\left(-\Gamma_{ph}(z)\right) = \Gamma_{ph}(0)\sigma_{pi} n_a \exp\left(-\sigma_{pi} n_a z\right), \tag{3}$$

where z represents the coordinate along the beam axis (with $z = 0$ corresponding to the point of entry of the beam in the gas cell) and $\Gamma_{ph}(z) = \Gamma_{ph}(0)\exp\left(-\sigma_{pi} n_a z\right)$ is the photon flux (photons/m^{2}s) along the beam axis. Integrating Eq. (3) from z = 0 to L, with L being the length of the gas cell, we obtain

$$n_i \approx n_e \approx \frac{\Gamma_{ph}(0)\sigma_{pi} n_a L}{2 c_s} = \frac{\Gamma_{ph}(0)\sigma_{pi} n_a L}{2 \times 10^4}\sqrt{\frac{A}{T_i}}, \tag{4}$$

where A is the mass of the gas species in atomic mass units and c_s is the ion-sound speed. We assumed the quasi-neutrality condition ($n_i \approx n_e$) and the Bohm condition at both ends of the gas cell wall. The recombination term, evaluated to be very small compared with the other terms, is neglected.

Figure 4 plots electron densities predicted by the 0 D (Eq. (1)) and 1 D (Eq. (4)) models using the BL7B beam photon flux shown in Fig. 2. Dashed curves represent densities at the probe position, 4 mm away from the beam axis. Because, in the present situation, the electron mean free path is comparable with the gas cell radius, the radial profile is given by the volume effect, $\propto r^{-2}$, i.e., $n_{e,probe} = \frac{1}{16} n_{e,beam}$. The density displays a local maximum near 20 eV and decays toward higher photon energy. Furthermore, the density becomes smaller than the local maximum by more than one order of magnitude in the energy range of more than 26 eV. This decrease is due to significant reductions in the photon flux and photoionization

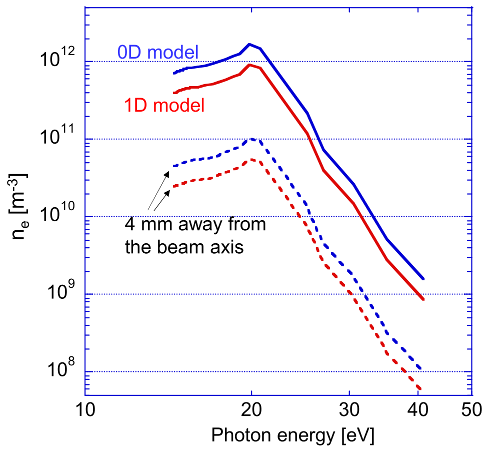

Fig. 4 Electron density predicted by the 0 D (Eq. (1), indicated by solid blue curves) and 1 D (Eq. (4), denoted by solid red curves) models as a function of photon energy. This is calculated using the photon flux of the beam in BL7B. Dashed curves represent density at the probe position, 4 mm away from the beam axis.

cross section [12] over this energy range. Therefore, the main contributions of the photon energy to the produced plasma density occur between 14.5 and 26 eV. Because the portion of photon energy in excess of the photoionization potential (14.5 eV) is imparted to electrons, the electron energy of the plasma ranges from 0.03 eV (a lower limit determined by the ambient temperature) to 11.5 eV. The actual Te value should be set to some value within this energy range through the relaxation process and should not exceed this range by much. The electron density is estimated from the probe measurement as

$$n_e \approx \frac{4 I_e}{e\, S\, v_{the}}, \tag{5}$$

where e, S, and v_{the} are the elementary charge, probe surface area, and electron thermal velocity, respectively. If we consider the aforementioned energy value as the electron temperature, as an example, Eq. (5) gives $n_e = 2.3 \times 10^{11}$, 1.2×10^{11}, 4.0×10^{10}, 1.7×10^{10}, and 1.2×10^{10} m^{-3} for 0.03, 0.1, 1.0, 5.5, and 11.5 eV, respectively. The obtained density values are close to the model predictions within experimental uncertainty for Te ranging from 0.03 to 1.0 eV; however, these values deviate substantially from the model predictions for Te = 5.5 and 11.5 eV. Although an accurate evaluation of the electron temperature and a more detailed investigation of the plasma characteristics remain, which will be conducted in the future, the present results suggest that the electron density is in the range of 10^{10} - 10^{11} m^{-3}.

In the present experiments, we do not observe clear Ar spectra with the used optical system even if the exposure time was increased up to 150 s. This is attributed to very low Ar emission in the present experiments. Further, we estimated that the photon flux of Ar emission received at optics in the present gas cell is 6–7 orders of magnitudes smaller than that in a nuclear fusion experiment device such as in Large Helical Device (LHD), where Ar spectra are measured routinely with an exposure time of 0.1 s. Therefore, increasing the exposure time by four orders of magnitude in the present experiments is insufficient to detect the spectra. (Details of the analysis will be presented elsewhere.)

A further development of the system may consider using the BL1U undulator beam line of UVSOR-III. The photon flux of BL1U is greater than that of BL7B by several orders of magnitude; therefore, a much higher plasma density is expected from the former, as shown in Table 1. Table 1 also indicates that the photoionization cross section, σ_{pi}, is substantially larger in UVSOR-III than in other devices. This is due to the ability to select the optimal photon energy (wavelength) in UVSOR-III, which maximizes σ_{pi}. Thus, substantial light emission from the gas will be available for spectral analysis. Additionally, the gas composition will be changed to include others such as neon, hydrogen, and also nitrogen and carbon monoxide to study photoinduced processes in biomolecules.

In summary, we made a first attempt at producing photoionized plasmas with the synchrotron light source in the VUV photon energy range using the BL7B beam line of UVSOR-III. As a first step, we used argon as the sample gas. The detection of electron current in the Langmuir probe measurement confirmed plasma production by photoionization. In terms of the plasma production process via photoionization, the probe current corresponds to an electron density of the order of 10^{10} to 10^{11} m^{-3}. These results demonstrate the capability of producing photoionized plasma in UVSOR-III in the VUV energy range. Additionally, in the future research, the system will be further developed using the undulator beam line BL1U to increase the plasma density for a more accurate evaluation of the plasma parameters and for the study of photoinduced processes in the divertor region of nuclear fusion reactors and in interstellar space in the context of astrobiology.

This work has been financially supported by JSPS KAKENHI grant No. 22K18272 and performed at the BL7B beamline of UVSOR Synchrotron Facility at the Institute for Molecular Science (IMS program 22IMS6869, 23IMS6673), Japan. One of the authors, M.K., is grateful to Mr. T. Itoh (Kitano Seisakusyo Corporation) for providing the technical support for fabricating the gas cell.

[1] M. Kotschenreuther *et al.*, Phys. Plasmas **14**, 072502 (2007).
[2] K. Sawada *et al.*, Contrib. Plasma Phys. **60**, e201900153, (2020).
[3] M. Kobayashi *et al.*, Contrib. Plasma Phys. **60**, e201900138 (2020).
[4] E.F. van Dishoeck *et al.*, Faraday Discussions **133**, 231 (2006).
[5] J. Takahashi *et al.*, Appl. Phys. Lett. **74**, 877 (1999).
[6] K. Kobayashi *et al.*, Astrobiology **21**, 1479 (2021).
[7] R.M. van der Horst *et al.*, J. Phys. D: Appl. Phys. **48**, 285203 (2015).
[8] C. Liu *et al.*, App. Phys. Expr. **15**, 036002 (2022).
[9] OPEN-ADAS, https://open.adas.ac.uk/
[10] M. Tanaka *et al.*, J. Synchrotron Radiat. **16**, 455 (2009).
[11] H. Ota *et al.*, J. Phys.: Conf. Ser. **2380** 012003 (2013).
[12] J.J. Yeh and I. Lindau, At. Data Nucl. Data Tables **32**, 1 (1985).